Tandem Mass Tag LC-MS/MS of Aqueous Humor From Individuals With Type 2 Diabetes Without Retinopathy Reveals Early Dysregulation of Synaptic Proteins

Mira M. Sachdeva,[1] Yoonjung Lee,[2,*] Eda K. Unlu,[1] Neslihan D. Koseoglu,[1] Eumee Cha,[1] Jiangxia Wang,[3] Christina R. Prescott,[4,**] Allen O. Eghrari,[4] and Chan Hyun Na[2]

[1]Retina Division, Wilmer Eye Institute, Johns Hopkins University School of Medicine, Baltimore, Maryland, United States
[2]Neurology, Institute for Cell Engineering, Johns Hopkins University School of Medicine, Baltimore, Maryland, United States
[3]Department of Biostatistics, Johns Hopkins University Bloomberg School of Public Health, Baltimore, Maryland, United States
[4]Cornea Division, Wilmer Eye Institute, Johns Hopkins University School of Medicine, Baltimore, Maryland, United States

Correspondence: Mira M. Sachdeva, Retina Division, Wilmer Eye Institute, Johns Hopkins University School of Medicine, 600 North Wolfe Street, Maumenee 748, Baltimore, MD 21287, USA; msachde4@jhmi.edu.

Current affiliation: *Institute for Systems Biology, Seattle, Washington, United States **Department of Ophthalmology, NYU Grossman School of Medicine, New York, New York, United States

Received: November 10, 2023
Accepted: February 19, 2024
Published: March 12, 2024

Citation: Sachdeva MM, Lee Y, Unlu EK, et al. Tandem mass tag LC-MS/MS of aqueous humor from individuals with type 2 diabetes without retinopathy reveals early dysregulation of synaptic proteins. *Invest Ophthalmol Vis Sci.* 2024;65(3):16. https://doi.org/10.1167/iovs.65.3.16

Purpose. An early neurodegenerative component of diabetic retinal disease (DRD) that precedes the vascular findings of clinically diagnosed diabetic retinopathy (DR) is increasingly being recognized. However, the relevant molecular mechanisms and biomarkers for early DRD are poorly defined. The purpose of this study was to uncover novel potential mediators of early diabetic retinal neuronal dysfunction through analysis of the aqueous fluid proteome in preclinical DR.

Methods. Aqueous fluid was collected from subjects with type 2 diabetes mellitus (DM) but no clinical DR and from nondiabetic controls undergoing routine cataract surgery. Preoperative spectral-domain optical coherence tomography of the macula was obtained. Tandem mass tag LC-MS/MS was performed to identify proteins differentially present in diabetic and control aqueous fluid, and proteins with >50% change and $P < 0.05$ were considered significant. Selected results were validated with western blot of human aqueous fluid samples.

Results. We identified decreased levels of proteins implicated in neuronal synapse formation and increased levels of inflammatory proteins in the aqueous fluid from patients with type 2 DM but no DR compared with controls. Of the differentially present synaptic proteins that we identified and confirmed with western blot, the majority have not previously been linked with DRD.

Conclusions. The proteomic profile of aqueous fluid from individuals with type 2 DM but no DR suggests that retinal neuronal dysfunction and inflammation represent very early events in the pathophysiology of DRD. These findings support the concept that diabetic retinal neurodegeneration precedes vascular pathology and reveal novel potential mediators and/or biomarkers warranting further investigation.

Keywords: proteomics, diabetic retinopathy, aqueous humor, neurodegeneration

Diabetic retinopathy (DR) remains the leading cause of blindness in working-age adults despite available treatments that target the retinal microvasculature at proliferative stages of disease. Although DR is diagnosed and staged based on its retinal vascular manifestations, patients with both type 1 and type 2 diabetes mellitus (DM) exhibit progressive thinning of the inner retina, including the retinal nerve fiber layer (RNFL) and ganglion cell layer (GCL)–inner plexiform layer (IPL) complex, on optical coherence tomography (OCT) imaging even prior to the onset of clinically evident DR, indicating an early neurodegenerative component to diabetic retinal disease (DRD).[1–4] Patients with DM but without DR also exhibit deficits in visual function, contrast discrimination, and retinal sensitivity on electroretinogram (ERG) and microperimetry testing.[5–8] Focal areas of delayed implicit time on multifocal ERG can predict localized DR development, suggesting that early neuronal changes may even contribute to subsequent vascular pathology.[8] Therefore, defining the molecular mediators of preclinical DRD, prior to the onset of DR, is critical to identifying appropriate therapeutic targets for early intervention and potential biomarkers for DR onset and/or progression.

Proteomics profiling of ocular fluid using mass spectrometry has provided insight into the pathophysiology of multiple ocular diseases, including choroidal melanoma[9], age-related macular degeneration[10], and DR.[11,12] However, most proteomics studies of ocular fluid in DR have utilized vitreous profiling in late stages of disease requiring surgical management (i.e., advanced proliferative DR [PDR]).[12–14] As aqueous fluid sampling typically confers lower risk and the aqueous protein composition has been shown to parallel the vitreous,[15] a few studies have investigated the aqueous

proteome in DR.[16–18] However, to date, unbiased profiling of proteomic changes in aqueous fluid early in the course of DRD (i.e., prior to clinical DR) has not been described. Using tandem mass tag (TMT) liquid chromatography–tandem mass spectrometry (LC-MS/MS), we compared the proteomic profile of aqueous fluid from individuals with type 2 DM without DR to the proteomic profile of aqueous fluid from controls in order to identify novel mediators and biomarkers for early preclinical DRD.

Methods

Subjects

Adults (>18 years of age) with and without type 2 DM undergoing evaluation for cataract extraction were prospectively recruited from the Wilmer Eye Institute at Johns Hopkins University School of Medicine from October 2020 through March 2021. Potentially eligible participants with type 2 DM were identified prior to their preoperative clinic visit by review of the electronic medical record, with the diagnosis of diabetes determined by the American Diabetes Association (ADA) laboratory criteria of fasting blood glucose >126 mg/dL or glycated hemoglobin (HbA1c) > 6.4% documented within the prior 12 months. Individuals with no documented history of DM in their electronic medical record were considered as potentially eligible controls. Participants with retinopathy on clinical exam were excluded from the study. Spectral-domain OCT (Heidelberg Engineering, Heidelberg, Germany) of the macula was performed preoperatively on each participant, and individuals with macular findings such as drusen, epiretinal membrane, and macular edema were excluded. Additional exclusion criteria included history of uveitis, glaucoma, optic neuropathy, high myopia (>5 diopters by refraction), other retinal pathology, neurodegenerative disease, and history of prior intraocular treatment (including laser or intravitreal injection) or surgery. This study adhered to the tenets of the Declaration of Helsinki and was approved by the Institutional Review Board at Johns Hopkins University School of Medicine. Written informed consent was obtained from each participant.

Retinal Thickness Measurement

Spectral-domain OCT images of the macula of the study eyes were obtained for each participant prior to cataract surgery using the SPECTRALIS instrument (Heidelberg Engineering) with the following scan acquisition parameters: dense volume scan (20° × 20°, roughly 6 × 6 mm) and 49 B-scans each spaced 120 µm apart, automatic real-time mean of 16, and high speed (512 A-/B-scans). All images were acquired by the same operator after pupillary dilation with 2.5% phenylephrine and 1% tropicamide. Images were evaluated using the Heidelberg Eye Explorer platform (HEYEX; Heidelberg Engineering). The automated segmentation tool was used to identify the boundaries of the retinal layers, and scan quality and segmentation accuracy were verified for each individual B scan by two masked graders (NDK, EC). Minor manual adjustments to the segmentation were made if needed. Retinal thickness values were obtained for the RNFL and GCL–IPL complex in each of the nine Early Treatment Diabetic Retinopathy Study (ETDRS) subfields: central fovea (1-mm diameter); superior, inferior, nasal, and temporal inner (ring centered on fovea with diameter of 3 mm); and outer (ring centered on fovea with diameter of 6 mm).

Serum HbA1c Measurement and Group Assignment

Serum was collected from each study participant in the preoperative area on the day of cataract surgery and HbA1c was measured. Point-of-care fasting blood glucose levels were also assessed by fingerstick. Individuals with a measured HbA1c > 6.4% on the day of cataract surgery were included in the diabetes group, and those with HbA1c ≤ 6.4% were analyzed as controls. Control participants were confirmed to have no prior or current history of anti-diabetic medication use.

Aqueous Fluid Sample Collection

Aqueous humor was collected from the operative eye in a sterile fashion at the beginning of each cataract surgery by one of two cataract surgeons (AOE, CRP). After the application of one or two drops of 0.5% proparacaine hydrochloride followed by 5% povidone iodine to the ocular surface and cleansing of the periocular skin with 10% povidone iodine, the operative eye was draped per standard sterile surgical protocol. An eyelid speculum was placed and aqueous fluid was manually aspirated from the anterior chamber using a sterile 30-gauge needle on a 3-mL syringe inserted through the limbus under the surgical microscope. Approximately 55 to 400 µL of aqueous fluid was collected per eye. The fluid samples were immediately transferred to Protein LoBind microcentrifuge tubes (Eppendorf, Hamburg, Germany) and placed on dry ice. Aqueous samples were stored at −80°C until further processing.

Sample Preparation for MS Analysis

One volume of 10-M urea in 50-mM triethylammonium bicarbonate (TEAB) was added to 100 µL of human aqueous fluid. A total of 36 samples were divided into three batches to conduct quantitative proteomic analysis using TMTpro 16plex (Electrophoretics Ltd., Surrey, UK). Each batch included one master pool (MP) and one quality control (QC) sample, which were prepared by combining an equal volume of proteins from all samples. The sample order for TMTpro labeling was randomized to minimize the effect of TMTpro channels. The MP sample was added to the 16th channel of each TMTpro experimental batch to normalize values from three different TMTpro experimental batches. The QC samples were included in each batch before reduction and alkylation to estimate technical and biological variations among the batches. For reduction and alkylation of the samples, 10-mM Tris (2-carboxyethyl) phosphine hydrochloride (TCEP, v/v) and 40-mM chloroacetamide (CAA, v/v) were added to the samples, and the mixtures were incubated for 1 hour at room temperature (RT). For digestion of the proteins, lysyl endopeptidase (Lys-C; FUJIFILM Wako, Richmond, VA, USA) was added (1:120) and incubated at 37°C for 3 hours. The sample solution was diluted to 2-M urea by adding four volumes of 50-mM TEAB. Subsequently, trypsin (1:50; Promega, Madison, WI, USA) was added to the samples, which were incubated at 37°C overnight. The samples were acidified to 1% trifluoroacetic acid and desalted using C18 stage tips (Empore; 3M, Maple-

Investigative Ophthalmology & Visual Science

wood, MN, USA). The peptide solution was vacuum dried and stored at −80°C until further use.

TMTpro 16plex reagents (Thermo Fisher Scientific, Waltham, MA, USA) were used for labeling of the peptides. The dried peptides were reconstituted in 100-mM TEAB, and 0.160 mg of each TMTpro reagent was reconstituted in 100% acetonitrile. Then, the peptides and TMTpro reagents were mixed and incubated for 1 hour at RT. The samples were quenched by adding 1/10 volume of 1-M Tris–HCl (pH 8.5) and incubating for 15 minutes at RT. The samples were pooled by proper volume and dried using a SpeedVac (Thermo Fisher Scientific) before pre-fractionation.

The peptides were reconstituted in 10-mM TEAB (pH 8.5) and loaded onto an Agilent 300Extend-C18 column (5 µm, 4.6 mm × 250 mm; Agilent Technologies, Santa Clara, CA, USA). An Agilent 1260 offline LC system (Agilent Technologies) consisting of a binary pump, ultraviolet detector, autosampler, and automatic fraction collector was used. The peptides were resolved using an increasing gradient of solvent B (10-mM TEAB in 90% acetonitrile, pH 8.5) at a flow rate of 0.3 mL/min. Ninety-six fractions were collected over a total run time of 150 minutes and were concatenated into 24 fractions. The concatenated samples were vacuum dried using a SpeedVac and stored at −80°C until further use.

MS Analysis

The MS analysis was conducted as described previously with minor modifications.[19] The fractionated samples were analyzed on an Orbitrap Fusion Lumos Tribrid Mass Spectrometer (Thermo Fisher Scientific) interfaced with an UltiMate 3000 RSLCnano liquid chromatography system (Thermo Fisher Scientific). The samples were reconstituted in 0.5% formic acid (FA) and loaded onto a trap column (Acclaim PepMap 100 C18, 5-µm, 100 µm × 20 mm; Thermo Scientific) at a flow rate of 8 µL/min. Peptides were separated on an analytical column (EASY-Spray PepMap RSLC C18, 2-µm, 75 µm × 500 mm; Thermo Fisher Scientific) at a flow rate of 0.3 µL/min using a linear gradient with mobile phases consisting of 0.1% FA in water and in 95% acetonitrile for 120 minutes. The mass spectrometer was operated in data-dependent acquisition (DDA) mode. The MS1 (precursor ions) scan range for a full survey scan was acquired from 300 to 1800 mass-to-charge ratio (m/z) in the top speed setting with a resolution of 120,000 at 200 m/z. The automatic gain control (AGC) target for MS1 was set as 1×10^6, and the maximum injection time was 100 ms. The most intense ions with charge states of 2 to 5 were isolated in a 3-second cycle, fragmented using higher energy collisional dissociation (HCD) fragmentation with 35% normalized collision energy, and detected at a mass resolution of 50,000 at 200 m/z. The AGC target for MS/MS (fragments) was set as 5×10^4, and the ion filling time was 100 ms. The precursor isolation window was set to 1.6 m/z with 0.4 m/z of offset. The dynamic exclusion was set to 30 seconds, and singly charged ions were rejected. Internal calibration was carried out using the lock mass option (445.1200025 m/z) from ambient air.

Proteomics Data Analysis

The data analysis was conducted as described previously with minor modifications.[19] Proteome Discoverer 2.4.1.15 (Thermo Fisher Scientific) was used for the identification and quantitation of proteins. The tandem mass spectrometry data were searched using SEQUEST algorithms against a human UniProt database that includes both Swiss-Prot and TrEMBL (released in December 2019) with common contaminant proteins. The search parameters used were as follows: (1) trypsin as a proteolytic enzyme (with up to two missed cleavages); (2) peptide precursor mass error tolerance of 10 ppm; (3) fragment mass error tolerance of 0.02 Da; (4) carbamidomethylation of cysteine (+57.02146 Da) and TMTpro tags (+304.207146 Da) on lysine and peptide N termini as fixed modifications; and (5) oxidation (+15.99492 Da) of methionine as a variable modification. The minimum peptide length was set to six amino acids. Peptides and proteins were filtered at a 1% false discovery rate (FDR) at the peptide–spectrum match (PSM) level using a percolator node and at the protein level using the protein FDR validator node, respectively. The protein quantification was performed with the following parameters. The most confident centroid option was used for the integration mode, whereas the reporter ion tolerance was set to 20 ppm. The MS order was set to MS2, and the activation type was set to HCD. Both unique and razor peptides were used for peptide quantification, whereas protein groups were considered for peptide uniqueness. The MS order for the protein quantification was set to MS2. Reporter ion abundance was calculated based on the signal-to-noise (S/N) ratio. The average reporter ion S/N threshold and co-isolation threshold were set to 50% and 30%, respectively.

Statistical and Bioinformatic Analysis of Proteomics Data

The statistical analysis of the MS data was performed using Perseus 1.6.7.0.[20] The protein abundance data from three batches of the TMTpro experiments were normalized by dividing the abundance data of the samples by those of the MPs included in each batch. Then, the reporter ion intensity values were divided by the median values of each protein, followed by $\log_2$ transformation of the values. Subsequently, the relative abundance values for each sample were subtracted by the median values of each sample and transformed into z-scores. Further normalization was conducted with the ComBat package in R (R Foundation for Statistical Computing, Vienna, Austria) to remove residual batch effects (Supplementary Fig. S1). After applying additional clinically relevant exclusion criteria, several samples were excluded from further analysis due to macular pathology identified on OCT imaging or glaucoma. Ultimately, 11 diabetes and 15 control samples were compared. The P values between the comparison groups were calculated using the Student's two-sample t-test. The fold change was calculated by dividing the mean value of one group by that of another group. Those proteins significantly up- or downregulated in the diabetes versus control samples were subject to Kyoto Encyclopedia of Genes and Genomes (KEGG) pathway and Gene Ontology (GO) analysis using the online DAVID resource. Interactome analysis was carried out by the STRING protein–protein interaction (PPI) databases (version 12).[21]

Western Blot

The protein concentration in each aqueous sample was measured using the Bradford assay (5000205; Bio-Rad, Hercules, CA, USA). One microgram of each sample was loaded onto an 8% Tris–glycine gel, separated by elec-

trophoresis at 120 volts, and transferred to a nitrocellulose membrane (1620115; Bio-Rad). Nitrocellulose membranes were assessed for equal loading using Ponceau S Staining Solution (Thermo Fisher Scientific) and then blocked with 5% non-fat dry milk for 1 hour at room temperature. Following blocking, membranes were incubated at 4°C overnight with the following primary antibodies: neural cell adhesion molecule 1 (NCAM1)/CD56 (3576S; Cell Signaling Technology, Danvers, MA, USA), SPARCL1 (AF2728; Bio-Techne, Minneapolis, MN, USA), LRRC4B (MAB69191; Bio-Techne), Neurexin1/2/3 (175003; Synaptic Systems, Göttingen, Germany), and SLITRK2 (4459; ProSci Inc., Poway, CA, USA). The membranes were then washed with Tris-buffered saline with 0.1% Tween 20 (TBST) and incubated in horseradish peroxidase (HRP)-conjugated secondary antibodies for 1 hour at RT. Finally, SuperSignal West Femto Maximum Sensitivity Substrate (34094; Thermo Fisher Scientific) was used to visualize the proteins on the membranes and blots imaged with an Amersham Imager 600 (GE Healthcare, Chicago, IL).

Additional Statistical Analyses

Demographic characteristics of the study participants were compared between the control and DM with no DR groups. The two-sample *t*-test was used for comparing continuous variables, and Fisher's exact test was used for the categorical variable of gender. Retinal thickness measurements of each layer in each subfield were directly compared using two-sample *t*-tests. For western blot data, intensities of the experimental bands and primary Ponceau bands for each sample were quantified using ImageJ (National Institutes of Health, Bethesda, MD, USA). Comparisons of the quantified normalized band intensities for each protein between control and diabetes samples were performed using two-tailed nonparametric Mann–Whitney *U* tests, with a significance cutoff of $P < 0.05$.

Results

A total of 46 individuals (30 without diabetes, 16 with type 2 DM but no retinopathy) undergoing routine cataract surgery initially consented to participate in this study. Preoperative serum samples were obtained from each study participant to directly measure HbA1c, and aqueous fluid was collected intraoperatively at the beginning of the case. Spectral-domain OCT of the macula was also obtained preoperatively. Eyes from which <120 µL of aqueous fluid was collected were excluded, so TMT LC-MS/MS was performed on aqueous fluid from 24 controls and 12 patients with type 2 DM without DR. TMT LC-MS/MS proteomics analysis of the aqueous fluid from these eyes identified a total of 1915 proteins.

We further applied additional clinically relevant exclusion criteria to minimize potential confounders. Eyes with macular pathology on preoperative OCT including epiretinal membrane, macular edema, or findings consistent with age-related macular degeneration (drusen, pigment epithelial detachments, choroidal neovascularization) were excluded from our analyses. Ultimately, our final comparison groups consisted of aqueous fluid from 15 control eyes and 11 eyes from individuals with type 2 DM but no DR. Baseline characteristics of these study participants are detailed in Table 1. There was no significant difference in the mean age ($P = 0.99$) or proportion of males versus females ($P = 0.23$) between the diabetes and control groups; however, as expected, serum glucose parameters were significantly different between the groups (Table 1). Interestingly, there was no significant difference in GCL–IPL or RNFL thickness in any of the ETDRS subfields between the diabetic and control eyes (Supplementary Table S1).

A total of 916 proteins were quantified among all of these samples and, using a significance cutoff of 50% change and $P < 0.05$, 49 proteins were differentially present in the aqueous of participants with type 2 DM without DR compared with controls, with 30 lower in the diabetes samples and 19 higher in the diabetes samples (Fig. 1). Of note, we used *P* values to assess for significant differences,

Table 1. Baseline Characteristics of Participants Included in the Final Proteomics Analysis

	Control ($n = 15$)	DM With No DR ($n = 11$)	*P*
Age (y), mean ± SD*	71 ± 5.9	71 ± 7.8	0.99
Sex, *n* (%)†			0.23
Male	5 (33)	7 (64)	
Female	10 (67)	4 (36)	
HbA1c (%), mean ± SD*	5.6 ± 0.48	7.4 ± 1.1	<0.001
Fasting glucose (mg/dL), mean ± SD*	96 ± 11	156 ± 65	0.002

* Compared with *t*-tests.
† Compared with Fisher's exact test.

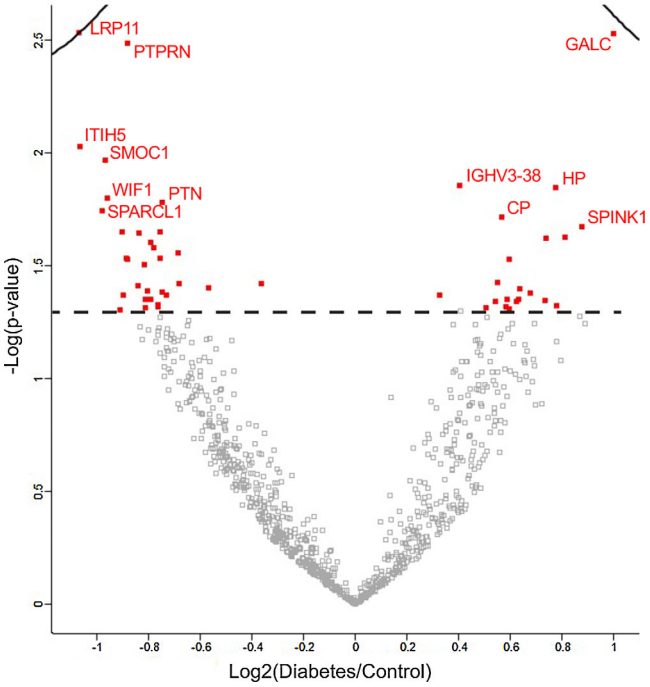

Figure 1. Volcano plot of differentially expressed proteins in aqueous samples from patients with type 2 DM but no DR compared with nondiabetic controls. The dashed line indicates a –log (*P* value) of 1.3 (i.e., $P = 0.05$), with proteins reaching the significance level of $P < 0.05$ highlighted in *red*. The 12 proteins with the lowest *P* values are specifically labeled in the diagram. Among those proteins, we further considered significant differential expression as a change of 50% or more compared with controls.

Table 2. Pathway Analyses of Differentially Present Proteins in Diabetic Aqueous Fluid

	KEGG Pathway	Proteins	*Q*
DM < control	Cell adhesion	SLITRK2, LRRC4B, NCAM1, NRXN2, NRXN3	0.0067
Control < DM	Complement and coagulation cascades	F9, F12, C2, KLKB1	0.0021
	GO Biological Process	**Proteins**	***P***
DM < control	Negative regulation of long-term synaptic potentiation	APP, APOE, PTN	0.00014
	Synaptic membrane adhesion	SLITRK2, SPARCL1, LRRC4B	0.00079
	Regulation of presynapse assembly	SLITRK2, APP, LRRC4B	0.0012
Control < DM	Zymogen activation	HGFAC, F9, F12, HP, HPR, KLKB1	5.8E-9
	Blood coagulation, intrinsic pathway	F9, F12, KLKB1	0.0036
	Blood coagulation	HGFAC, F9, F12, KLKB1	0.0046

Table 3. List of Proteins Decreased in Aqueous Fluid From Patients With Type 2 DM Without DR Compared With Nondiabetic Controls

Protein Symbol	Accession No.	PSMs, *n*	Log_2 (Diabetes/Control)	*P*
LRP11	Q86VZ4	15	−1.0682	0.00294734
ITIH5	C9J2H1	260	−1.06389	0.00940005
SPARCL1	Q14515	331	−0.979128	0.01816854
SMOC1	Q9H4F8	32	−0.968447	0.01083378
WIF1	Q9Y5W5	476	−0.959184	0.01587048
LRRC4B	Q9NT99	25	−0.908756	0.04958839
DNAJC3	Q13217	48	−0.902022	0.02246312
NRXN3	A0A0U1RQC5	200	−0.897062	0.04279076
MXRA5	Q9NR99	53	−0.886224	0.02947678
LTBP3	Q9NS15	101	−0.883669	0.0296811
PTPRN	Q16849	13	−0.881238	0.00329503
APP	P05067	432	−0.839239	0.03879181
CXCL12	P48061	20	−0.836833	0.02265896
SERPINE2	P07093	56	−0.815413	0.03127015
NRXN2	G5E9G7	99	−0.813994	0.0445841
PTGDS	P41222	1367	−0.812555	0.04861161
COL18A1	P39060	123	−0.802717	0.04090063
NPTX2	P47972	44	−0.79383	0.04448668
SEZ6	Q53EL9	53	−0.792179	0.02502995
MGAT5	Q09328	46	−0.778332	0.02633965
APOE	P02649	698	−0.764915	0.04801202
HS6ST1	O60243	15	−0.762676	0.04729334
PPM1L	Q5SGD2	16	−0.756002	0.02949171
DNASE2	O00115	30	−0.754059	0.02243417
PTN	P21246	39	−0.747733	0.0166303
GM2A	P17900	42	−0.746948	0.04149254
SLITRK2	Q9H156	27	−0.731305	0.04281934
ECRG4	C9JRR0	9	−0.686826	0.02786891
NCAM1	P13591	122	−0.682916	0.03786431
MYOC	Q99972	304	−0.568208	0.03980338

as correction for multiple testing with calculated *Q* values did not reach statistical significance for the proteins identified, likely due to our small sample size. KEGG and GO analyses using DAVID algorithms revealed that components of cell adhesion pathways, specifically synapse assembly (SLITRK2, LRRC4B, NCAM1, NRXN2, NRXN3, and SPARCL1), were significantly decreased in samples from diabetic participants and that components of the complement and coagulation cascades were significantly increased in the diabetic samples (Table 2). Additional proteins that were decreased in the aqueous fluid of diabetic participants included other regulators of synaptic structure and/or function (SMOC1 and NPTX2), Wnt signaling (WIF1), protein aggregation (APP), and components of lipoprotein signaling (APOE and LRP11) (Tables 3, 4). We also conducted STRING protein interactome analyses to identify key proteins and nodes among the components in the enriched pathways (Supplementary Fig. S2). Comparison of our results with published MS-based proteomics studies of vitreous humor from eyes with advanced PDR revealed several findings consistent with those analyses.[11,12] However, although we were able to detect angiogenic molecules known to play a role in the pathophysiology of the retinal microvascular complications of DR, including VEGFA, KDR, ANGPTL1, and ANGPTL7, there was no difference in abundance of these proteins in the aqueous fluid from eyes with type 2 DM but no DR (Supplementary Table S2). Importantly, we also confirmed the absence of diabetic macular edema in these eyes on OCT as described above.

Given the early retinal neurodegenerative component of DRD, we decided to further investigate expression of the downregulated synaptic/cell adhesion proteins revealed by

Table 4. List of Proteins Increased in Aqueous Fluid From Patients With Type 2 DM Without DR Compared With Nondiabetic Controls

Protein Symbol	Accession No.	PSMs, *n*	Log_2 (Diabetes/Control)	*P*
GALC	P54803	19	0.997868	0.00297037
SPINK1	P00995	7	0.878716	0.02119191
APOA4	P06727	935	0.811807	0.02379962
P4HB	P07237	55	0.77752	0.04765956
HP	P00738	916	0.773926	0.01429091
CD44	H0YCV9	17	0.73643	0.02388746
F12	P00748	104	0.732702	0.04500388
IL1RAP	Q9NPH3	26	0.678735	0.04176668
KLKB1	P03952	139	0.634563	0.04036454
HGFAC	Q04756	46	0.631225	0.0447332
C2	P06681	280	0.622164	0.04594307
SAA2–SAA4	A0A096LPE2	67	0.597202	0.02958081
CRISP3	J3KPA1	7	0.596769	0.04910096
HPX	P02790	2023	0.587741	0.04483736
AMBP	P02760	307	0.58165	0.0484652
CP	P00450	2104	0.567177	0.01930545
F9	P00740	53	0.549677	0.03772593
MCAM	P43121	33	0.542565	0.04589021
A1BG	P04217	450	0.506941	0.04897224

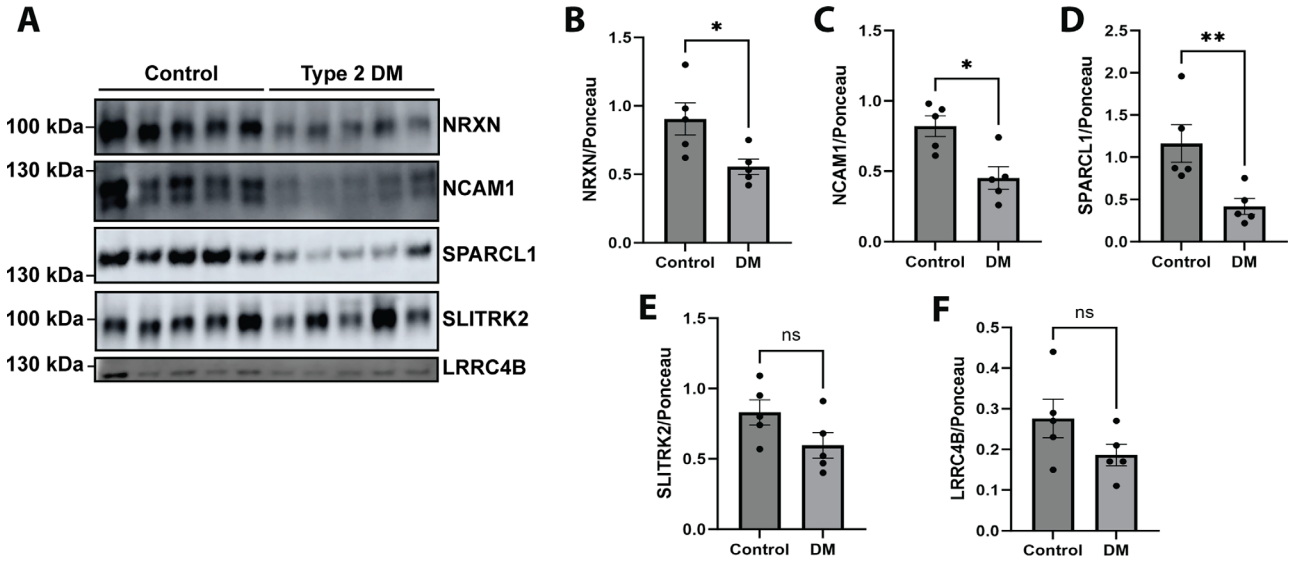

Figure 2. Decreased expression of synaptic proteins in aqueous fluid from eyes from patients with type 2 DM without DR compared with nondiabetic controls. Aqueous fluid (1 µg total protein/lane) from the eyes of five individuals with type 2 DM but no DR and five nondiabetic control patients was evaluated by western blot (**A**). Ponceau staining was used to confirm equal total protein loading per sample and to normalize the intensity of the probed bands for quantification. The diabetic aqueous samples had significantly decreased levels of NRXN (**B**), NCAM1 (**C**), and SPARCL1 (**D**). For SLITRK2 (**E**) and LRRC4B (**F**), the decrease in protein levels in the diabetic samples did not reach statistical significance ($P = 0.09$ and $P = 0.17$, respectively). $^{*}P < 0.05$, $^{**}P < 0.01$.

our proteomics analyses in the aqueous humor of control and diabetic patients. Due to the lack of a reliable antibody to distinguish neurexin (NRXN) isoforms, we used a pan-NRXN antibody that detects all isoforms of NRXN1, NRXN2, and NRXN3. We were able to detect the synaptic proteins NRXN, NCAM1, SPARCL1, LRRC4B, and SLITRK2 in human aqueous humor by western blot (Fig. 2). NRXN, NCAM1, and SPARCL1 were confirmed to be significantly decreased in aqueous fluid from eyes of patients with diabetes but no DR compared with controls (Fig. 2). For SLITRK2 and LRRC4B, western blot quantification showed a decrease in mean levels of these proteins in the diabetic aqueous that did not reach statistical significance ($P = 0.09$ and $P = 0.17$, respectively), but may with a larger cohort.

Discussion

The majority of proteomics studies of DRD have analyzed the vitreous humor in advanced PDR, with limited investigation of the aqueous proteome and earlier stages of disease. In one study describing proteomic and metabolomic profiling of aqueous fluid from individuals with different stages of systemic diabetes, eyes with other retinal pathology such as age-related macular degeneration were included.[22] Recently, an ocular fluid analysis including patients with DM but no DR using aptamer-based proteomics was reported.[18] To our knowledge, our study is the first to utilize an unbiased proteomics approach to compare aqueous fluid proteins in eyes from individuals with type 2 DM but without DR or other retinal pathology and controls in order to identify novel pathways and mediators of early preclinical DRD. This is also the largest cohort of aqueous samples from diabetic patients evaluated using TMT-based LC-MS/MS to quantitatively analyze different protein levels in the samples with higher accuracy.

We identified downregulation of several cell adhesion and synaptic proteins in the diabetic aqueous samples and used western blot to confirm decreased expression of NRXN, NCAM1, and SPARCL1 in aqueous fluid from participants with type 2 DM but no DR. Levels of SLITRK2 and LRRC4B were also decreased in aqueous fluid from diabetic patients, but these differences did not achieve statistical significance with our western blot sample size. Of these proteins, NCAM1 has the strongest known link with DR. Loss-of-function animal models suggest that NCAM may contribute to retinal neuronal development and response to injury, and decreased levels of polysialylated NCAM have been associated with retinal ganglion cell (RGC) degeneration in a streptozotocin-induced diabetic mouse model.[23,24] The potential contributions of the other downregulated synaptic proteins we identified to the pathophysiology of early DRD remain unexplored. Interestingly, recent studies have demonstrated decreased NRXN expression in the brain and pancreas of diabetic mouse models, suggesting a potential link between NRXNs and DM.[25,26] The NRXNs represent a complex family of proteins that regulate synapse assembly and neurotransmitter release in the brain, but their roles in the retina are incompletely defined.[27,28] SPARCL1 has been identified as a secreted protein that can induce synaptogenesis in RGCs.[29] LRRC4B (also known as netrin-G ligand-3) and SLITRK2 are transmembrane proteins important for normal brain development that play roles in excitatory synapse formation in the hippocampus, although their functions in the retina are unknown.[30–32] The potential roles of these proteins in DRD represent a path for future investigation.

Several of the additional proteins differentially identified in our proteomics analysis or their associated biological processes, namely Wnt signaling (WIF1), protein aggregation (APP), and lipoprotein signaling (APOE), have already been implicated in the pathophysiology of DR. WIF1 overexpression has been shown to improve markers of mitochondrial function in a diabetic mouse model.[33] Aberrant APP processing has been suggested to play a role in early DRD based on proteomics analysis of postmortem retinal tissue from diabetic patients.[34] APOE deficiency in mice increases susceptibility to retinal neurodegeneration and vasculopathy in the context of a high-fat diet.[35]

Our findings that aqueous fluid from individuals with type 2 DM harbors a significant decrease in proteins associated with synapse structure and function even prior to clinically evident DR support the emerging concept that diabetic retinal neurodegeneration represents an early feature of DRD and suggests novel potential mediators or biomarkers for further investigation. In addition, we found that these changes in the ocular proteome were detected in the absence of inner retinal thinning on macular OCT, suggesting that retinal neuronal synaptic dysfunction may even precede the now well-described structural changes in preclinical DRD. It is also possible that subtle RNFL and/or GCL–IPL thinning was present in the eyes included in this study but differences between the control and diabetes groups did not reach statistical significance due to the sample size.

Moreover, we observed no difference in protein levels of vascular endothelial growth factor A (VEGFA), the most well-characterized marker and mediator of DR, or other proangiogenic factors in the aqueous fluid from diabetic eyes at this early stage, suggesting that the retinal neuronal dysfunction in diabetes may precede retinal vascular pathology. These findings contribute to the emerging paradigm shift in our understanding of DRD that has led to efforts to redefine DRD to include both neural and visual function components in addition to the classic vascular changes. In addition, our findings that aqueous fluid from eyes of individuals with type 2 DM demonstrate higher levels of components of the complement and coagulation cascades even in the absence of clinically evident DR indicate that inflammation is an early event.

The strengths of our study include rigorous assessment of diabetes status by direct HbA1c serum measurement at the time of aqueous fluid collection, as well as confirmation of the absence of other retinal disease not only by clinical exam but also by OCT. This is a critical point, as other studies have demonstrated that the aqueous proteome in both nonexudative (dry) and exudative (wet) age-related macular degeneration differs from controls.[10,36] Moreover, although for practical reasons proteomics studies of vitreous fluid collected intraoperatively during pars plana vitrectomy often use eyes with macular pathology including epiretinal membranes and macular holes as controls for comparison with PDR, it is possible and very likely that the proteomic intraocular milieu in eyes with macular pathology may not be "normal." In this study, we were able to confirm the absence of any structural macular pathology on OCT in both our control and diabetes comparison groups, allowing for a more direct assessment of changes in the aqueous proteome associated specifically with diabetes. Additional strengths of our study include the unbiased approach for peptide identification via TMT LC-MS/MS, as well as our confirmatory western blot results, which further validate the rigor of our proteomics dataset.

Limitations of this analysis include the small sample size and, as with any proteomic profiling study, its correlative nature, precluding any conclusions regarding causative links between the proteins identified and early DRD. Also, because we collected aqueous fluid samples during routine cataract surgery, all individuals included had a cataract causing some degree of visual symptoms. Although the presence of a cataract in these eyes may have influenced the protein composition of the aqueous humor, it would be presumed that this confounder would be similar across eyes in both the control and diabetes groups. Finally, inclusion of an additional group of individuals with frank DR in future longitudinal studies of the aqueous humor profile in DM would provide important insights into the potential clinical relevance of the proteomic changes we identified here to the onset and progression of DRD. Overall, our findings

Investigative Ophthalmology & Visual Science

strengthen the concept of an early retinal neuronal dysfunction component of DRD and suggest potential candidate mediators for further investigation.

Acknowledgments

The authors thank Melissa Collins for her expertise with the OCT image acquisition.

Supported by a grant from the National Institutes of Health (K08EY029766 to MMS), a National Institutes of Health High-End Instrumentation Grant (S10OD021844), and a Clinical Scientist Development Award from the Doris Duke Foundation (to MMS). MMS hold a Wilmer Rising Professorship.

Disclosure: **M.M. Sachdeva**, None; **Y. Lee**, None; **E.K. Unlu**, None; **N.D. Koseoglu**, None; **E. Cha**, None; **J. Wang**, None; **C.R. Prescott**, None; **A.O. Eghrari**, None; **C.H. Na**, None

References

1. Carpineto P, Toto L, Aloia R, et al. Neuroretinal alterations in the early stages of diabetic retinopathy in patients with type 2 diabetes mellitus. *Eye (Lond)*. 2016;30:673–679.
2. Sohn EH, van Dijk HW, Jiao C, et al. Retinal neurodegeneration may precede microvascular changes characteristic of diabetic retinopathy in diabetes mellitus. *Proc Natl Acad Sci USA*. 2016;113:E2655–E2664.
3. van Dijk HW, Verbraak FD, Kok PHB, et al. Decreased retinal ganglion cell layer thickness in patients with type 1 diabetes. *Invest Ophthalmol Vis Sci*. 2010;51:3660.
4. van Dijk HW, Verbraak FD, Kok PHB, et al. Early neurodegeneration in the retina of type 2 diabetic patients. *Invest Ophthalmol Vis Sci*. 2012;53:2715–2719.
5. van Dijk HW, Verbraak FD, Stehouwer M, et al. Association of visual function and ganglion cell layer thickness in patients with diabetes mellitus type 1 and no or minimal diabetic retinopathy. *Vision Research*. 2011;51:224–228.
6. McAnany JJ, Park JC, Lim JI. Visual field abnormalities in early-stage diabetic retinopathy assessed by chromatic perimetry. *Invest Ophthalmol Vis Sci*. 2023;64:8.
7. Park JC, Chen Y-F, Liu M, Liu K, McAnany JJ. Structural and functional abnormalities in early-stage diabetic retinopathy. *Curr Eye Res*. 2020;45:975–985.
8. Han Y, Bearse MA, Jr, Schneck ME, Barez S, Jacobsen CH, Adams AJ. Multifocal electroretinogram delays predict sites of subsequent diabetic retinopathy. *Invest Ophthalmol Vis Sci*. 2004;45:948–954.
9. Velez G, Nguyen HV, Chemudupati T, et al. Liquid biopsy proteomics of uveal melanoma reveals biomarkers associated with metastatic risk. *Mol Cancer*. 2021;20:39.
10. Qu S-C, Xu D, Li T-T, Zhang J-F, Liu F. iTRAQ-based proteomics analysis of aqueous humor in patients with dry age-related macular degeneration. *Int J Ophthalmol*. 2019;12:1758–1766.
11. Schori C, Trachsel C, Grossmann J, Zygoula I, Barthelmes D, Grimm C. The proteomic landscape in the vitreous of patients with age-related and diabetic retinal disease. *Invest Ophthalmol Vis Sci*. 2018;59:AMD31–AMD40.
12. Santos FM, Ciordia S, Mesquita J, et al. Proteomics profiling of vitreous humor reveals complement and coagulation components, adhesion factors, and neurodegeneration markers as discriminatory biomarkers of vitreoretinal eye diseases. *Front Immunol*. 2023;14:1107295.
13. Loukovaara S, Nurkkala H, Tamene F, et al. Quantitative proteomics analysis of vitreous humor from diabetic retinopathy patients. *J Proteome Res*. 2015;14:5131–5143.
14. Sen S, Udaya P, Maheshwari JJ, et al. Comparative proteomics of proliferative diabetic retinopathy in people with type 2 diabetes highlights the role of inflammation, visual transduction, and extracellular matrix pathways. *Indian J Ophthalmol*. 2023;71:3069–3079.
15. Balaiya S, Zhou Z, Chalam KV. Characterization of vitreous and aqueous proteome in humans with proliferative diabetic retinopathy and its clinical correlation. *Proteomics Insights*. 2017;8:117864181668607.
16. Xiao H, Xin W, Sun LM, Li SS, Zhang T, Ding XY. Comprehensive proteomic profiling of aqueous humor proteins in proliferative diabetic retinopathy. *Transl Vis Sci Technol*. 2021;10:3.
17. Chiang S-Y, Tsai M-L, Wang C-Y, et al. Proteomic analysis and identification of aqueous humor proteins with a pathophysiological role in diabetic retinopathy. *J Proteomics*. 2012;75:2950–2959.
18. Wolf J, Rasmussen DK, Sun YJ, et al. Liquid-biopsy proteomics combined with AI identifies cellular drivers of eye aging and disease in vivo. *Cell*. 2023;186:4868–4884.
19. Jang Y, Pletnikova O, Troncoso JC, et al. Mass spectrometry–based proteomics analysis of human substantia nigra from Parkinson's disease patients identifies multiple pathways potentially involved in the disease. *Mol Cell Proteomics*. 2023;22:100452.
20. Tyanova S, Temu T, Sinitcyn P, et al. The Perseus computational platform for comprehensive analysis of (prote)omics data. *Nat Methods*. 2016;13:731–740.
21. Szklarczyk D, Gable AL, Lyon D, et al. STRING v11: protein–protein association networks with increased coverage, supporting functional discovery in genome-wide experimental datasets. *Nucleic Acids Res*. 2019;47:D607–D613.
22. Fortenbach CR, Skeie JM, Sevcik KM, et al. Metabolic and proteomic indications of diabetes progression in human aqueous humor. *PLoS One*. 2023;18:e0280491.
23. Murphy JA, Franklin TB, Rafuse VF, Clarke DB. The neural cell adhesion molecule is necessary for normal adult retinal ganglion cell number and survival. *Mol Cell Neurosci*. 2007;36:280–292.
24. Lobanovskaya N, Jürgenson M, Aonurm-Helm A, Zharkovsky A. Alterations in the polysialylated neural cell adhesion molecule and retinal ganglion cell density in mice with diabetic retinopathy. *Int J Ophthalmol*. 2018;11:1608–1615.
25. Yokokawa T, Kido K, Sato K, Hayashi T, Fujita S. Altered expression of synaptic proteins and adhesion molecules in the hippocampus and cortex following the onset of diabetes in nonobese diabetic mice. *Physiol Rep*. 2023;11:e15673.
26. Mosedale M, Egodage S, Calma RC, Chi N-W, Chessler SD. Neurexin-1α contributes to insulin-containing secretory granule docking. *J Biol Chem*. 2012;287:6350–6361.
27. Südhof TC. Synaptic neurexin complexes: a molecular code for the logic of neural circuits. *Cell*. 2017;171:745–769.
28. Fuccillo MV, Földy C, Gökce Ö, et al. Single-cell mRNA profiling reveals cell-type-specific expression of neurexin isoforms. *Neuron*. 2015;87:326–340.
29. Kucukdereli H, Allen NJ, Lee AT, et al. Control of excitatory CNS synaptogenesis by astrocyte-secreted proteins Hevin and SPARC. *Proc Natl Acad Sci USA*. 2011;108:E440–E449.
30. Woo J, Kwon S-K, Choi S, et al. Trans-synaptic adhesion between NGL-3 and LAR regulates the formation of excitatory synapses. *Nat Neurosci*. 2009;12:428–437.
31. Lee H, Shin W, Kim K, et al. NGL-3 in the regulation of brain development, Akt/GSK3b signaling, long-term depression, and locomotive and cognitive behaviors. *PLoS Biol*. 2019;17:e2005326.
32. Beaubien F, Raja R, Kennedy TE, Fournier AE, Cloutier J-F. Slitrk1 is localized to excitatory synapses and promotes their development. *Sci Rep*. 2016;6:27343.

33. Zou J, Tan W, Liu K, Chen B, Duan T, Xu H. Wnt inhibitory factor 1 ameliorated diabetic retinopathy through the AMPK/MTOR pathway-mediated mitochondrial function. *FASEB J*. 2022;36:e22531.
34. Sundstrom JM, Hernández C, Weber SR, et al. Proteomic analysis of early diabetic retinopathy reveals mediators of neurodegenerative brain diseases. *Invest Ophthalmol Vis Sci*. 2018;59:2264–2274.
35. Cao X, Guo Y, Wang Y, et al. Effects of high-fat diet and Apoe deficiency on retinal structure and function in mice. *Sci Rep*. 2020;10:18601.
36. Rinsky B, Beykin G, Grunin M, et al. Analysis of the aqueous humor proteome in patients with age-related macular degeneration. *Invest Ophthalmol Vis Sci*. 2021;62:18.

Investigative Ophthalmology & Visual Science